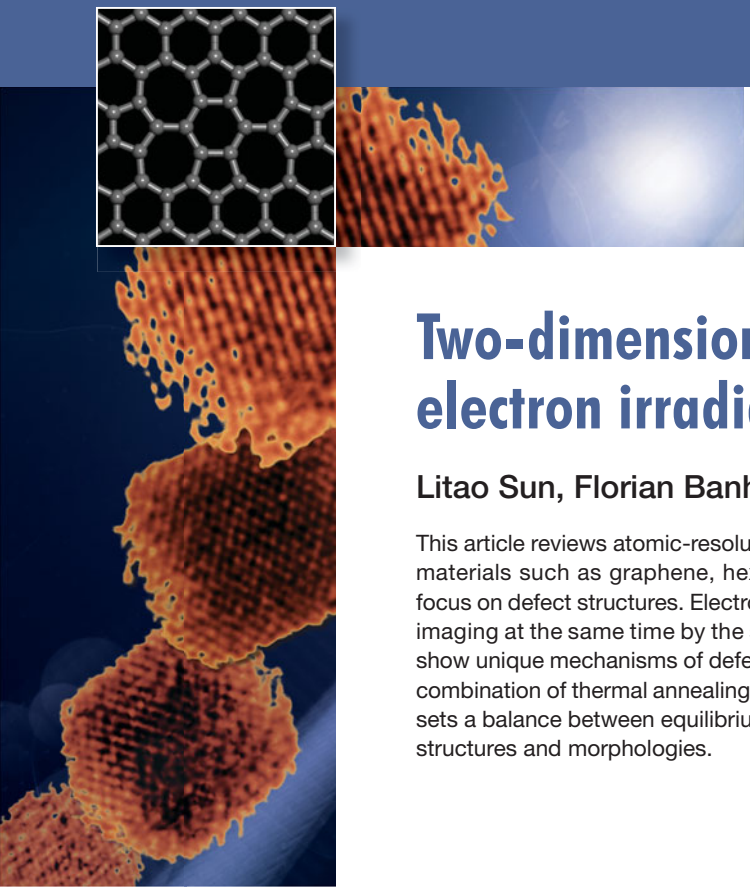


Two-dimensional materials under electron irradiation

Litao Sun, Florian Banhart, and Jamie Warner

This article reviews atomic-resolution *in situ* electron microscopy studies of two-dimensional materials such as graphene, hexagonal boron nitride, and metal dichalcogenides with a focus on defect structures. Electron irradiation allows defect formation and atomic-resolution imaging at the same time by the same electron beam. Two-dimensional hexagonal lattices show unique mechanisms of defect reconstruction that do not appear in other materials. The combination of thermal annealing and irradiation, both adjustable in the electron microscope, sets a balance between equilibrium and nonequilibrium and allows for the generation of new structures and morphologies.

Atomic imaging of two-dimensional materials

Two-dimensional (2D) systems such as graphene have been among the most studied materials in the past 10 years. Stable 2D materials are highly anisotropic crystals with strong covalent in-plane bonding and weak van der Waals interlayer bonding. The unusual properties of graphene, namely, its ballistic electron conductance and its high tensile strength, have made it one of the most studied materials of our time.[1,2] However, the absence of a bandgap in graphene motivates the search for alternative 2D materials. Hexagonal boron nitride (h-BN) and the chalcogenides of molybdenum or tungsten are the most prominent examples that have been synthesized and characterized in detail.[3–5] A common feature of many 2D materials is a hexagonal lattice in which the atoms are arranged in a honeycomb structure.

Transmission electron microscopy (TEM) has turned out to be ideally suited for studying 2D materials. A large number of *in situ* experiments have been carried out in which the beam served not only for imaging but also for irradiation. The creation of point defects has been monitored in real time and with atomic resolution. The particular appeal of TEM studies of 2D materials is that the reconstruction of the lattice occurs in the 2D atomic plane and can, in many cases, be seen without any projection artifacts. Hence, a detailed picture of the atomic arrangement of defective materials becomes visible. Striking TEM images of point defects in graphene, recorded at a lateral resolution smaller than the bond length of carbon, leave almost no room for uncertain interpretation. Novel mechanisms of lattice reconstruction have been discovered in *in situ* irradiation experiments, such as transformations between different polygons.[6–8]

In addition to a detailed understanding of radiation-induced defects and their influence on the properties of 2D sheets, the design of new structures has become feasible. Irradiation-induced structural changes can be achieved and characterized in real time and at the full lateral resolution of the instrument. On one hand, modern TEM instruments achieve an imaging resolution of better than 1 Å, which is less than the distance between atoms in solids. This provides the possibility of imaging individual atoms and their migration under electron irradiation. On the other hand, electron beams can be focused onto spots of less than 1 Å, which allows use of the beam as tweezers to manipulate materials at the single atom level.[9–11]

Detailed *in situ* electron irradiation experiments of 2D materials have been carried out,[12–18] and the transmission electron microscope has become a useful tool for studying the structural stability of materials and creating new nanostructures.[15,19–27] Not only the formation but also the annealing of defects can be controlled in such irradiation experiments if high-temperature specimen stages are used. The reconstruction of vacancies in carbon nanostructures, which has turned out to be the basis for many surprising phenomena, requires temperatures above

Litao Sun, SEU-FEI Nano-Pico Center, Key Lab of MEMS of Ministry of Education, Southeast University, China; slt@seu.edu.cn
Florian Banhart, IPCMS, UMR 7504 CNRS, University of Strasbourg, France; florian.banhart@ipcms.unistra.fr
Jamie Warner, Department of Materials, University of Oxford, United Kingdom; jamie.warner@materials.ox.ac.uk
DOI: 10.1557/mrs.2014.303

© 2015 Materials Research Society

https://doi.org/10.1557/mrs.2014.303 Published online by Cambridge University Press

200–300°C.[28,29] Although detailed pictures of radiation effects and defects in graphene have been obtained, the information available about defects in other 2D materials is still rather limited. Therefore, many inorganic 2D materials are still awaiting investigation, and the field is certainly ripe for new discoveries and surprises. In this article, the atomic structural evolution of 2D materials such as graphene, h-BN, and metal dichalcogenides under *in situ* electron irradiation and the mechanisms of defect reconstruction are reviewed.

Defects in graphene

Graphene, as the most prominent 2D material, was the first in which irradiation effects were studied. The rise of aberration-corrected TEM instruments allowed the imaging of each carbon atom in a graphene sheet and, hence, the achievement of a precise and unambiguous picture of the atomic arrangement in defects such as single or multiple vacancies.

Even if no atoms are removed, structural defects can be created by the electron beam. A Stone–Wales (SW) defect is an example that is formed by an in-plane 90° rotation of a C–C bond (**Figure 1**a–d). Four adjacent hexagons are transformed into two pentagons and two heptagons. The kinetic barrier for such a bond rotation is 9–10 eV, whereas the barrier of the reverse transformation is only 5 eV.[30] Both barriers are less than the calculated displacement threshold energy of 18–22 eV,[31,32] such that both transformations can occur below the displacement threshold.[33] A remarkable and stable defect structure in graphene can be formed from six SW rotations to yield a closed-loop structure,[9] shown in Figure 1e–h. An aberration-corrected TEM (AC-TEM) image of this defect is shown in Figure 1h. No atoms are lost, with only a core of seven hexagons rotated by 30° to form a miniature grain boundary. The detailed mechanisms by which this structure is produced are not yet fully clear, but it is likely that the structure results from the relaxation of a more complex defect into this stable configuration. The schematic presented in Figure 1e–h is for illustrative purposes to help in understanding the final closed-loop structure. It has also been reported that bond rotations play an important role in other defect reconstructions, as discussed in the next subsection.

Traditionally, vacancy formation is thought to occur through direct sputtering of atoms from the lattice by high-energy electrons. However, in graphene, this process is much more complicated than the simple picture of knock-on damage. It was long thought that using electrons accelerated at 80 kV would not damage graphene because the maximum energy transferred to a carbon atom is below the theoretical displacement energy. However, recent work showed that vacancies are formed using an accelerating voltage of 80 kV.[18] Surprisingly, the sputtering cross-section at 80 kV also depends on the beam current density.[18] The origin of defect creation in graphene at 80 kV is likely due to the high mobility of adatoms on the surface of graphene, allowing them to interact with graphene within the intense electron beam irradiation, thereby disrupting the regular sp^2 hexagonal network. Any perturbation to the pristine structure, such as SW rotations or self-interstitials, can generate bonds that are weaker and therefore atoms that can be sputtered at a lower energy to form vacancies. Calculations of sputtering cross-sections in graphene are also complicated by the fact that vacancies can be created and then easily quenched through the trapping of mobile surface C adatoms, allowing them to disappear before being registered in the image. Therefore, the total number of missing atoms counted at any one time can vary and might not reflect the total number of atoms sputtered in a specific time interval. Further work is needed to clarify this issue in more detail. One thing is clear: The damage mechanisms in graphene at energies below 100 kV are more complicated than simple knock-on damage from one electron hitting one carbon atom to cause ejection and vacancy formation.[18]

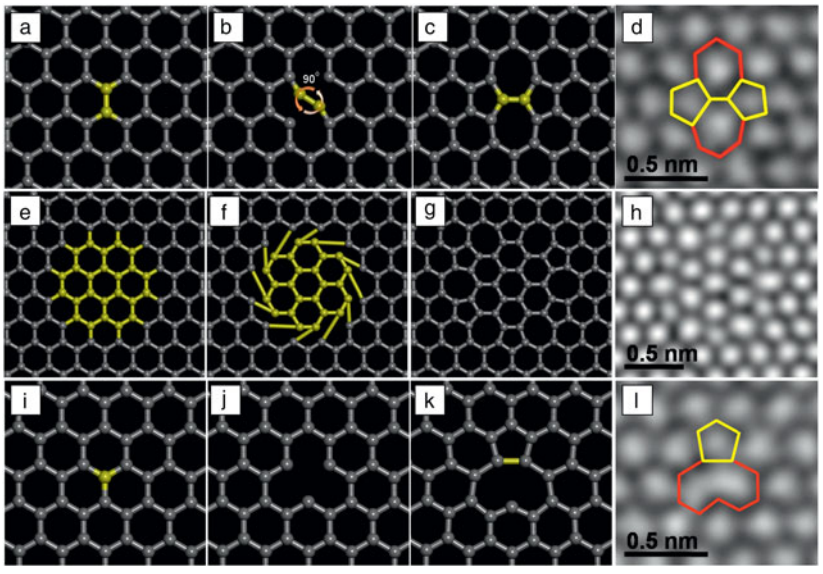


Figure 1. Stone–Wales (SW) rotation and single-vacancy defects in graphene: (a–c) Atomic models showing the formation of a SW defect by an in-plane 90° rotation of a C–C bond. Atoms indicated in yellow show the rotated bond. (d) Aberration-corrected transmission electron microscopy (AC-TEM) image of a SW defect. (e–g) Atomic models showing the formation of a miniature grain boundary by a rotation of a seven-hexagon core. Yellow atoms indicate the rotated region. (h) AC-TEM image of a closed-loop defect. (i–k) Atomic models showing the formation of a reconstructed single vacancy. The yellow atom is the one removed, and the yellow bond indicates the reconstructed bond. (l) AC-TEM image of a reconstructed single-vacancy defect. For (d) and (l), red lines indicate heptagons, and yellow lines indicate pentagons. (a–d) Reproduced with permission from Reference 8. © 2013 Royal Society of Chemistry. (e–h) Reproduced with permission from Reference 9. © 2012 Nature Publishing Group. (i–l) Reproduced with permission from Reference 34. © 2013 American Chemical Society.

https://doi.org/10.1557/mrs.2014.303 Published online by Cambridge University Press

To understand complex defect structures in graphene, it is important to start with an overview of the basic defects that form the building blocks of defects in graphene. The simplest type is a single vacancy (SV). To minimize its energy, the SV undergoes a Jahn–Teller distortion, which leads to the saturation of two of the three dangling bonds around the missing atom (Figure1i–l). The Jahn–Teller distortion lowers the overall energy of the system by removing electronic degeneracies. This leads to the formation of a pentagon and a nonagon[33,34] (the nonagon has a dangling bond). The energy barriers among the three Jahn–Teller reconstructions are small, and therefore, it is expected that under an electron beam at 80 kV, the structure should easily rotate among these three configurations. This has the effect of averaging out the reconstruction in a TEM image, giving a symmetric appearance to the defect. Recent *in situ* TEM work showed that, in many cases, a Jahn–Teller reconstructed SV locks into a specific orientation and remains stable for up to one minute.[34] It is proposed that this is due to either hydrogen attaching to the dangling bond of the C atom or one of the atoms within the vacancy being N. Further work is under way to shed more light on this stable SV configuration. SVs can frequently be observed at 80 kV and are stable for periods of up to several minutes, but are quenched by the trapping of mobile adsorbates. Most of the time, these are C atoms, but sometimes, they can be other elements, such as N, Fe, or Si.[35–37]

Divacancies (DVs) are also commonly observed and are able to reconstruct the lattice such that no dangling bonds occur. They appear in several configurations of slightly different energy, as shown in **Figure 2**. They are created either when two migrating SVs coalesce or when an atom next to an existing SV is displaced. Because of the absence of open bonds, a DV is energetically more favorable than two SVs.[38] Under 80 kV electron beam irradiation, the DV oscillates between the three configurations shown in Figure 2, but with a higher percentage of time spent in the DVs with +1 and +2 bond rotations (atomic models in Figure 2e–f).

Larger and more complex defect configurations can be formed by removing more atoms. Generally, vacancies with an even number of missing atoms, where all bonds are saturated, are energetically favored over an odd number of vacancies with at least one open bond.[39] In the extreme case, graphene with a large density of vacancies can appear as a 2D carbon glass, which can be described as a coherent quasi-amorphous membrane composed of sp^2-hybridized carbon atoms.[18,40,41]

Recent work on tetravacancies in graphene (i.e., four atoms missing) revealed that the most common structures under electron beam irradiation involve either linear defects along the armchair direction or bond rotations.[61] **Figure 3**a–e shows atomic models of how four atoms can be removed from the graphene lattice, considering only nearest-neighbor types without any bond rotations. Of these structures, only the structures in Figure 3a and 3d have been observed. Figure 3f–g shows AC-TEM images of the two most common tetravacancy structures in graphene: (f) the armchair defect (cf. Figure 3d) and (g) the tetravacancy with three bond rotations, the formation of which is schematically shown in Figure 3h–m. As in the case of the DV structure, continual electron beam irradiation at 80 kV causes successive bond rotations that enable transitions to a variety of structures.[40]

One-dimensional line defects such as dislocations have also been observed in graphene under electron irradiation.[42–44] Because of graphene's two-dimensional nature, only dislocations

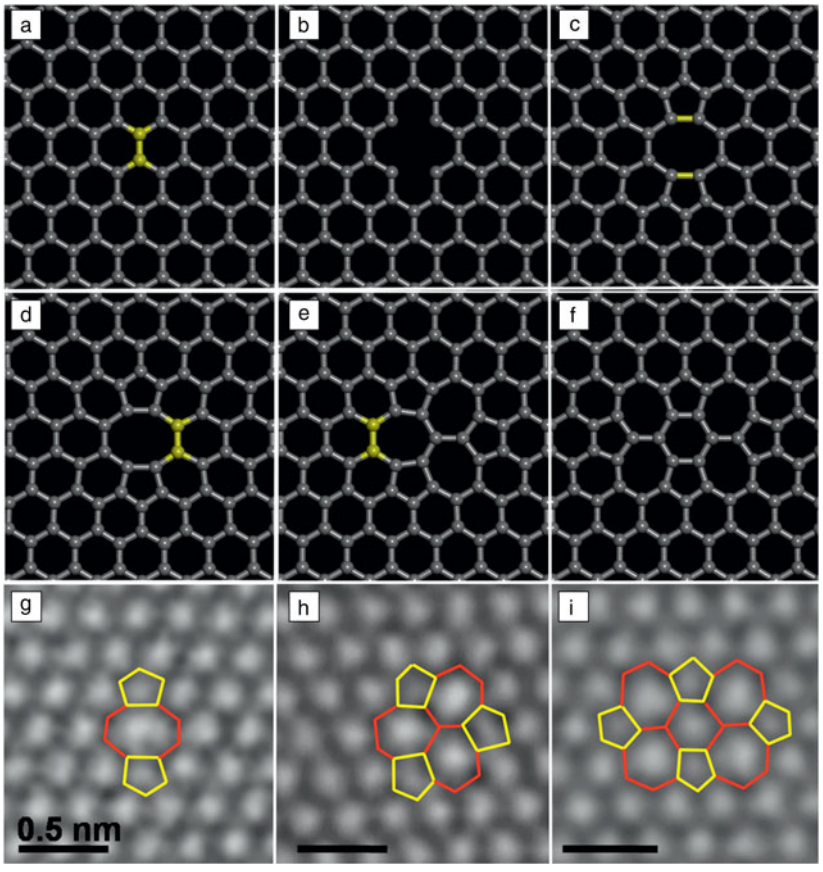


Figure 2. Divacancy (DV) defects in graphene: (a–c) Atomic models showing the removal of two C atoms (indicated with yellow) and bond reconstruction to form the 5–8–5 (pentagon–octagon–pentagon) DV (indicated with yellow). (d–f) Atomic models showing how (d) a 5–8–5 DV transforms into (e) a 555–777 DV by one bond rotation (yellow atoms in panel d) and then into (f) a 5555–6–7777 DV by a second bond rotation (yellow atoms in panel e). (g–i) Aberration-corrected transmission electron microscope images of DV structures shown in corresponding atomic models above each panel. Red lines indicate an octagon in (g) and heptagons in (h) and (i); yellow lines indicate pentagons. Reproduced with permission from Reference 9. © 2012 Nature Publishing Group.

https://doi.org/10.1557/mrs.2014.303 Published online by Cambridge University Press

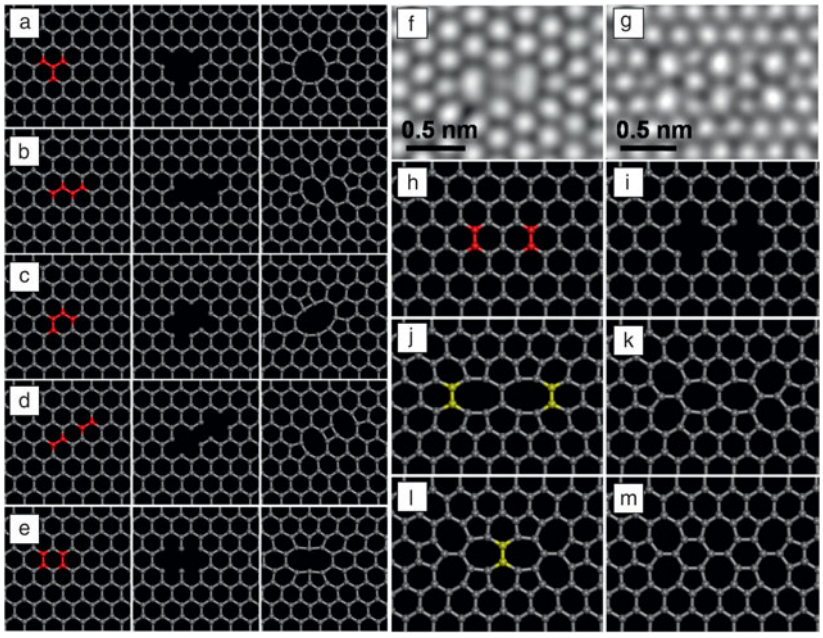


Figure 3. Tetravacancy defects in graphene: (a–e) Atomic models showing how the removal of four carbon atoms in close proximity leads to tetravacancies without any bond rotations. Red atoms indicate those to be removed. Sequences run horizontally. (f–g) Aberration-corrected transmission electron microscope images of the most common tetravacancy structures in graphene: (f) the armchair defect (cf. Figure 3d) and (g) the tetravacancy with three bond rotations. (h–m) Atomic models showing how the tetravacancy structure in panel g can be constructed. Red indicates atoms to be removed; yellow indicates bond rotations. Reproduced with permission from Reference 61. © 2014 American Chemical Society.

of the edge type appear.[45] They can be constructed by the removal of a zigzag chain of carbon atoms.[46] The role of the dislocation core is played by a pentagon–heptagon pair that appears at the end of the strip. Dislocations can migrate within the graphene sheet either by bond rotations along the glide plane (glide) or by the addition or removal of two carbon atoms (creep). The strain induced by the addition of dislocations causes out-of-plane distortions in the graphene sheet, buckling the structure. Electron beam irradiation can cause these ripples to propagate within graphene sheets.

Intense irradiation removes a large number of atoms from a small area, causing the formation of a hole with unsaturated bonds around its circumference.[23–25,47–49] The edges of the holes can be zigzag, armchair, or reconstructed lines.[47,50–53] Defective edges also appear[54] because of the sustained removal of atoms from perfect edges. Furthermore, upon exposure of two adjacent holes to electron irradiation, the bridge between the edges often becomes narrower, such that only a single chain of carbon atoms is left before the bridge breaks.[19,20,48,55] Further types of defects in graphene have been described in specialized reviews.[6,8]

Previous experiments on electron irradiation[25,28] also indicated that a large fraction of irradiation-induced damage in graphene can anneal *in situ*, especially at temperatures higher than 300°C, where SVs become mobile. Two important mechanisms govern defect annealing:[56] the saturation of dangling bonds by the formation of non-hexagonal rings and the migration of carbon interstitials or vacancies, followed by Frenkel pair recombination (i.e., a recombination of interstitial and vacancy).

As described earlier, the formation of pentagon–nonagon rings after atom removal is a simple reconstruction that saturates two of three dangling bonds.[34] The reconstruction causes strain in the surrounding lattice. At the same time, non-hexagonal rings induce local curvature in the graphene sheet, creating hillocks or trenches to accommodate strain.[57,58] In addition, the formation of pentagons causes positive curvature in graphene and leads to bowl-shaped structures or even closed spherical cages.[59]

It is worth noting that bond rotation can reconstruct most types of defects in graphene. The barrier of bond rotation is smaller than that for displacement, so bond rotation occurs at a much higher frequency under electron irradiation. The transformation among three different DV configurations[8,60] is shown in Figure 2d–f. A bond rotation of the yellow bond in Figure 2d leads to transformation from a 5–8–5 (a DV configuration with 5–8–5 membered rings, as shown in Figure 2d) to a 555–777 configuration (another DV configuration with three 5-membered rings and 7-membered rings, as shown in Figure 2e). Another rotation in Figure 2e results in a transformation to a DV of the 5555–6–7777 type (a complex DV configuration, as shown in Figure 2f). Similarly, bond rotations can also govern the transformation between different configurations of a tetravacancy[61] or induce the migration of vacancies[60] or grain boundaries.[62]

Most types of defects can act as potential doping sites when they trap other atoms.[63,64] The effects of foreign atoms on the electronic properties of graphene depend on the charge transfer between the atom and the graphene, which is governed by the type of bonding.[65] Various bonding configurations (such as on top of a carbon atom or on top of the center of a hexagon) are possible. *In situ* observation of the migration of atoms as a function of temperature allows the determination of which types of bonding can occur.[37,66–72] Because of the locally increased reactivity of the π-electron system,[70,73,74] reconstructed defects serve as reactive sites even if all covalent bonds are saturated. At the same time, the strain field around reconstructed defects can lead to an attractive interaction over a scale of 1–2 nm between the defect and a foreign atom migrating on the surface.[70] As shown in **Figure 4**, a tungsten atom can jump back and forth between two defective sites at a distance of 0.5–1.4 nm. A biaxial strain of 1% in the graphene lattice increases the adsorption energy for transition-metal adatoms by 0.06–0.16 eV, depending on the metal species and the adsorption site.

https://doi.org/10.1557/mrs.2014.303 Published online by Cambridge University Press

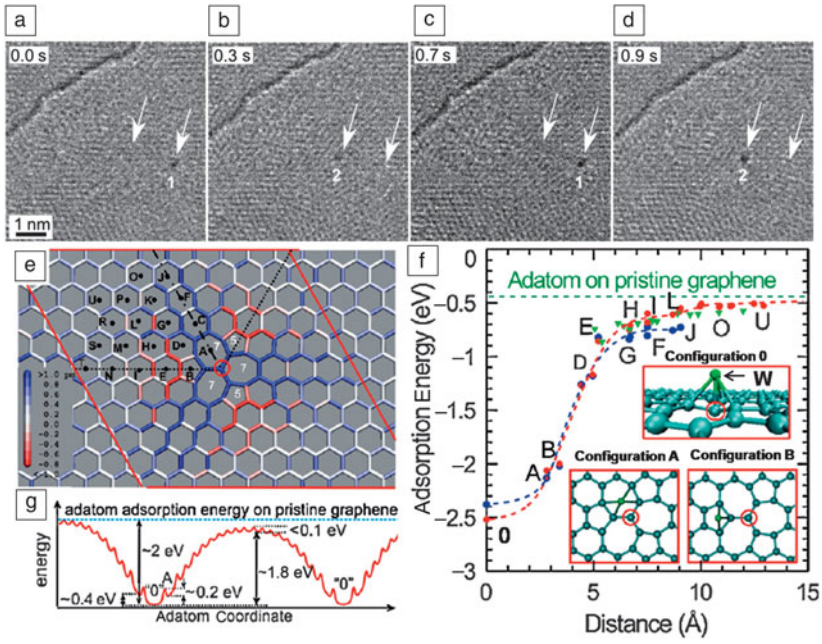


Figure 4. Jumping of a W atom on the surface of few-layer graphene at 480°C: (a–d) Repeated jumping between two trapping sites (denoted by white arrows and 1 and 2) at a distance of 1.5 nm. (e) The 555-777 defect naturally produces a strain field in its vicinity. The bonds are colored according to an increase (blue) or decrease (red) in the bond length (given in picometers). The letters indicate all nonequivalent position of W atoms in the configurations. The red lines outline the (10 × 10) simulation cell. (f) Adsorption energy of a W adatom near a 555–777 defect as a function of the separation between the adatom and the middle of the defect (circled atom in [e]) obtained from a 10 × 10 simulation cell (red) and a 7 × 7 supercell (blue). The letters indicate W adatom position in (e). The insets show the positions of the adatoms in the lowest energy configurations. The energy drop (approximately 2 eV) results from the stretched carbon–carbon bonds at the defects where a higher electron density is available for forming new bonds with the adatom. (g) Energy of a W adatom in various positions on a graphene sheet with two 555–777 defects. The potential well for the adatom can explain the attraction between the adatom and pinning centers, which is seen in transmission electron microscopy observations as a repeated jumping of the W atom between two trapping sites. Reproduced with permission from Reference 70. © 2010 American Physical Society.

Foreign atoms can also be incorporated into graphene as substitutional impurities. In this case, the impurity atom replaces one or two carbon atoms. However, most foreign atoms are located slightly off the layer because of the greater bond lengths between carbon and other atoms.[75] Substitutional dopants are expected to be very stable because of their strong covalent bonding with the graphene lattice; nevertheless, they can migrate under electron irradiation, especially when the foreign atoms are located at graphene edges.[72] **Figure 5** shows the jumping of a Fe atom between two sites.[37] Figure 5a–b shows the Fe atom moving between different graphene sublattice sites, whereas Figure 5e–f shows the rotation of the dopant position through a change in the lattice site.[37] Figure 5i–l shows an initial vacancy in graphene that traps a mobile Fe atom to form a dopant. The Fe atom then switches configurations from bonding to four nearest carbon atoms to bonding to three, induced by electron beam irradiation at 80 kV.[37] Similar behavior has been observed for silicon atoms.[90]

Defect formation in graphene has been demonstrated to have spatial control to within 10 nm using *in situ* electron beam irradiation within an AC-TEM. By controlling the beam current density and exposure time, it is possible to produce either small MVs and DVs or large complex vacancy structures.[9] The small MVs and DVs act as traps for mobile metal atoms, such as Fe, to form single atom dopants covalently bonded in the lattice.[37] This demonstrates how *in situ* electron beam irradiation can be used to engineer the doping of graphene with 10 nm precision.

Defects in other inorganic 2D materials

Structurally related 2D inorganic materials such as h-BN and transition metal dichalcogenides (TMDs) have attracted much interest recently because of their remarkable properties, which differ considerably from those of graphene. These 2D materials are alternatives to graphene and show promise for applications in electronics, optoelectronics, catalyses, or energy storage devices. Despite the technological potential of inorganic 2D materials, electron irradiation inside the TEM has been applied in only a few studies. The effects of irradiation in inorganic 2D materials are much more complex than those in graphene because of their complex layered structures with several atomic layers per monolayer in some of these 2D materials, and the fact that more than one element is involved, leaving a larger variety of possible defect structures. Although data on the responses of such inorganic 2D materials to electron irradiation are scarce, we analyze the available experimental results here and try to draw conclusions on the general behavior of inorganic 2D materials under irradiation.

h-BN layers have the closest structural similarity to graphene. *In situ*, as well as *ex situ*, experiments in AC-TEM instruments have shown that boron atoms are displaced more often than nitrogen atoms,[12,16,76,77] because the threshold energy for knock-on displacements of B atoms (74 keV) is smaller than that of N atoms (84 keV) in defect-free h-BN monolayer sheets.[78] Single boron vacancies, but not single nitrogen vacancies, have been created under irradiation at an electron energy of 80 keV.[16,76] It is interesting that the selective sputtering of B atoms has also been observed at an electron energy of 120 keV,[12] although both species should be displaced, such that other mechanisms might also be involved.

Because B–B and N–N bonds are less favorable than B–N bonds, SW defects or reconstructed vacancies were not expected in h-BN. Most recently, however, pentagon–heptagon (5–7) and square–octagon (4–8) defects were

https://doi.org/10.1557/mrs.2014.303 Published online by Cambridge University Press

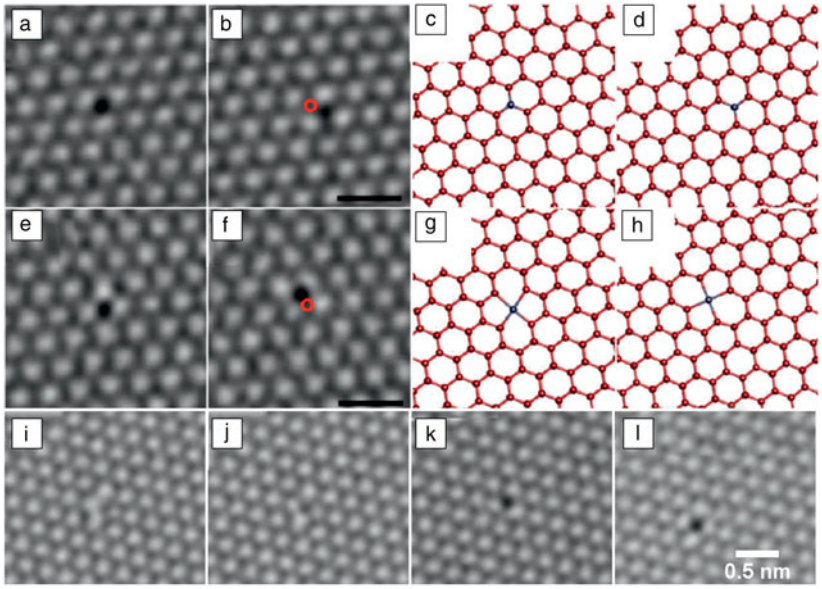


Figure 5. Migration of Fe atoms under electron irradiation: (a–b) Jumping of an Fe atom between adjacent single vacancy sites. Scale bar indicates 0.5 nm and (c–d) corresponding atomic models. Blue atom indicates the location of the Fe atom. (e–f) Changing of an Fe atom between two divacancy sites. Scale bar indicates 0.5 nm and (g–h) corresponding atomic models. Blue atom indicates the location of the Fe atom. Red circles show the location of the dopant atom in the previous frame. (i–l) Time series of images (10 s between images) showing an Fe atom hopping into a vacancy in graphene and switching its bonding configuration. Reproduced with permission from Reference 37. © 2013 American Chemical Society.

observed by TEM.[79,80] Cretu et al. observed the *in situ* formation of 4–8 defects at high temperature (~1000 K) under 60 keV electrons.[79] Surprisingly, the 4–8 defects appeared to be stable with homoelemental B–B and N–N bonds, although these bonds should be energetically less favorable than B–N bonds. Apparently, this compensates the energy from possible open bonds and the strain energy in the reconstructed defect. Further studies, however, are necessary to clarify this issue. The defects could also be mobilized along the armchair direction by the gliding of atomic rows, induced by high temperature and electron irradiation.[79] As more defect structures are found, further studies will be required to fully understand the formation and evolution of multivacancies in h-BN sheets under electron irradiation.

In situ electron irradiation with a higher dose was found to give rise to the formation of larger triangular holes in BN because unsaturated nitrogen atoms at the edges could also be displaced by 80 keV electrons, resulting in the growth of the vacancy.[16,76,81] Although holes with other shapes have also been observed in few-layer h-BN sheets,[81] triangular holes dominate in monolayer h-BN under 80 keV irradiation. It is interesting to note that the internal edges of the triangular holes show a nitrogen-terminated zigzag configuration because of the higher threshold energies of N atoms.

Another interesting experiment involved the introduction of C atoms into BN sheets by electron irradiation such that BCN sheets were created.[82,83] Wei et al. used paraffin wax as a carbon source to create BCN sheets in a transmission electron microscope operating at 300 kV.[82] Under electron irradiation, carbon atoms were split from hydrocarbon molecules. The electron energy was sufficiently high to knock both B and N atoms from the h-BN lattice. These vacancies were immediately filled by C atoms. The behavior of BCN sheets under electron irradiation shows features of the behaviors of both graphene and h-BN because triangular vacancy aggregates as well as irregular holes appear.[84] Electron-irradiation-assisted doping appears to indicate a pathway to the design and synthesis of in-plane heterostructures. The upscaling of *in situ* electron irradiation studies (e.g., by exposing large areas to electron irradiation in a dedicated facility) could be used to fabricate 2D heterostructures, such as BCN with pre-defined electronic properties, on an industrial level.

TMDs represent another interesting class of 2D materials. Here, a unit cell consists of three atomic layers. Early experiments[85,86] showed that chalcogenides exposed to electron irradiation are most likely deformed through the removal of sulfur atoms by knock-on displacements. Recent experiments on MoS_2[13,17] showed that both single and double sulfur vacancies can be generated under irradiation of 80 keV electrons. **Figure 6**a shows a high-resolution TEM image of a single S vacancy in a monolayer of MoS_2.[17] The types of defects can be distinguished by analyzing the intensity profile and comparing it with the intensity profiles of simulated vacancy images.[17] Further studies of defect evolution under electron irradiation with different exposure times demonstrated that the average vacancy generation rate of single S vacancies was 10^{10} $cm^{-2}s^{-1}$ when the beam current density was several amperes per square centimeter, in agreement with theoretical predictions.[13,17] Similar to graphene and h-BN, vacancies can be filled with other atomic species that are deliberately introduced onto the specimen.[13] It is interesting that the structure can also be transformed between semiconducting (2H) and metallic (1T) phases in single MoS_2 sheets under electron irradiation. This transformation can be achieved even when no substitutional atoms are present and, moreover, at an electron energy of 60 keV, where no beam-irradiation-induced displacements are expected.[87]

Under continuous irradiation, S vacancies diffuse and agglomerate and then form an extended line defect that can be described as a row of SVs (Figure 6b). After prolonged exposure to the electron beam, the lines expand and span over two neighboring rows of the S sublattice to form wider defect lines.[14] Additional irradiation gives rise to the formation of large holes in MoS_2 sheets, as shown in Figure 6c, but the holes have no regular shape. During growth of the holes, the bridges between adjacent holes narrowed to nanoribbons (Figure 6d).

https://doi.org/10.1557/mrs.2014.303 Published online by Cambridge University Press

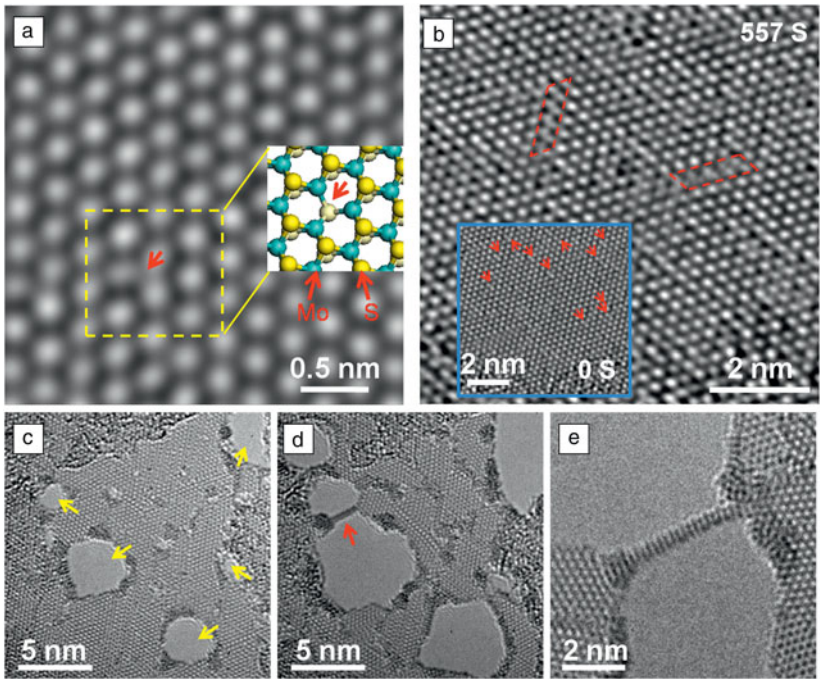


Figure 6. Electron irradiation damage of monolayer MoS_2 under 80 keV electron irradiation: (a) Atomic structure and high-resolution transmission electron microscope image of a single sulfur vacancy. The inset is the atomic model, where the blue atoms are molybdenum atoms and the others are sulfur atoms. (b) Sulfur vacancies (denoted by arrows) diffuse and agglomerate and then form an extended line defect (highlighted by dotted lines). The inset is the same area before electron irradiation. (c) Holes (denoted by yellow arrows) without a distinct shape formed under continuous irradiation. (d) Growth of holes, where the connecting regions between the adjacent holes are narrowed into nanoribbons (denoted by red arrow), which are robust under 80 keV irradiation. (e) The ribbons exhibit a different crystalline structure than MoS_2 ribbons. (a–b) Reproduced with permission from Reference 17. © 2013 Nature Publishing Group. (c–e) Reproduced with permission from Reference 15. © 2013 Nature Publishing Group.

The ribbons showed high crystalline perfection, unlike any other known molybdenum disulfide ribbons (Figure 6e). It is interesting to note that the ribbons were much more robust under electron irradiation than large MoS_2 sheets.[15] Through a combination of first-principles calculations and TEM imaging simulations, it was shown that such <1-nm ribbons were Mo_5S_4 crystals.[15] Further calculations indicated that the ribbons were semiconductors with an indirect band gap of 0.77 eV. Recently, based on further experimental evidence, Lin et al. offered new insight into ribbon properties and structure.[26] *In situ* electrical measurements had demonstrated that the ribbons were metallic, which was inconsistent with previous work. After further analysis, Lin et al. concluded that a model with the MoS stoichiometry more closely matched the experimental observations. They also fabricated WS, MoSe, and WSe nanowires by 80 keV electron irradiation.[26]

To our knowledge, no electron irradiation studies of other 2D materials have been published to date. Most recently, the responses of van der Waals heterostructures (such as stacked graphene and MoS_2 layers) to electron irradiation were studied by two groups.[88,89] The results indicated that irradiation damage could be lessened by placing a MoS_2 layer on a single layer of graphene. Furthermore, the damage of single-layer MoS_2 under 60 keV electron irradiation could also be reduced by encapsulation of the single-layer MoS_2 between graphene layers.[88] Sandwiched graphene/MoS_2/graphene structures were also found to be protected from radiation damage by 80 keV electrons.[89] It was estimated that the total vacancy formation rate was reduced by a factor of 600 in the sandwiched configuration[89] compared to that in a freestanding MoS_2 layer.

Conclusions and outlook

The transmission electron microscope projects the structure of monoatomic sheets directly onto the image plane. No loss of information in the third dimension occurs because the third dimension either does not exist (graphene) or consists of only two or three atomic planes (chalcogenides). As a result, the formation of defects, even at the single-atom level, can be observed *in situ*. Similar studies, in which the atomic coordinates of a particular defect configuration can be determined with high accuracy, have never been possible in three-dimensional materials.

Since aberration-corrected electron microscopy became available, structural defects in graphene have been studied in detail, and a large variety of defect configurations are known. Other 2D materials, however, are just now attracting the interest of electron microscopists, so it can be expected that these materials will be studied in more detail in the near future. *In situ* electron microscopy is indispensable since it allows both defect generation by electron irradiation and defect observation at the same time. Common defect configurations have already been observed, such that the understanding of defect formation and annealing will allow for the identification of more general principles regarding reconstruction in hexagonal 2D materials. The availability of electron beam spot sizes smaller than the distance between atoms in solids allows the structure of 2D materials to be tailored with atomic precision. Because defects in hexagonal monoatomic lattices show unique reconstruction behavior, the removal of atoms allows for the creation of new morphologies and, accordingly, new types of nanoparticles in one, two, and three dimensions.

Acknowledgments

The authors are indebted to T. Xu, K. Yin, X. Xie, Y. Zhou, Y. Shen, A. Krasheninnikov, J.A. Rodríguez-Manzo, O. Cretu, M. Terrones, P.M. Ajayan, H.Kroto, R. Ruoff, J. Kotakoski, H. Zhang, D. Yu, X. Wang, W. Guo, G. Zhang, J. Wang, Z. Ni, C. Jin, J. Li, and Y. Gan for scientific collaborations in the

https://doi.org/10.1557/mrs.2014.303 Published online by Cambridge University Press

areas covered in this review. L.S. gratefully acknowledges support from the National Basic Research Program of China under Grant 2011CB707601; the National Natural Science Foundation of China under Grants 61274114, 51420105003, 113279028, and 51071044; and the Natural Science Foundation and Qing Lan Project of Jiangsu Province under Grants BK2011592 and BK2012024. J.W. thanks the Royal Society for support. F.B. is indebted to the French Agence Nationale de Recherche for financial support through Grants NANOCONTACTS and NANOCELLS (ANR12 BS1000401).

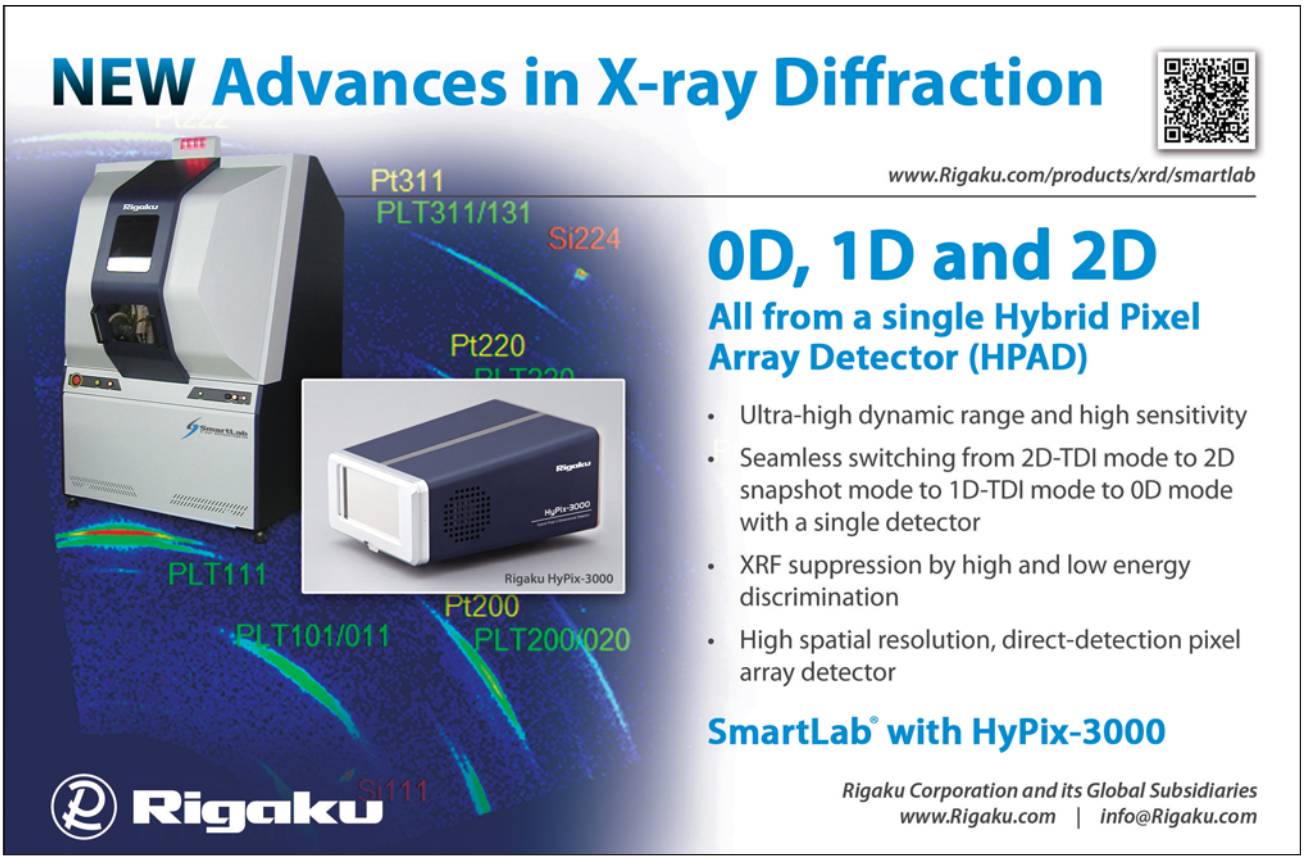
References

1. K.S. Novoselov, V.I. Falko, L. Colombo, P.R. Gellert, M.G. Schwab, K. Kim, *Nature* **490**, 192 (2012).
2. A.K. Geim, *Science* **324**, 1530 (2009).
3. W.-Q. Han, L. Wu, Y. Zhu, K. Watanabe, T. Taniguchi, *Appl. Phys. Lett.* **93**, (2008).
4. C. Lee, Q. Li, W. Kalb, X.-Z. Liu, H. Berger, R.W. Carpick, J. Hone, *Science* **328**, 76 (2010).
5. Z. Zeng, Z. Yin, X. Huang, H. Li, Q. He, G. Lu, F. Boey, H. Zhang, *Angew. Chem. Int. Ed.* **50**, 11093 (2011).
6. F. Banhart, J. Kotakoski, A.V. Krasheninnikov, *ACS Nano* **5**, 26 (2010).
7. A.V. Krasheninnikov, K. Nordlund, *J. Appl. Phys.* **107**, 071301 (2010).
8. A.W. Robertson, J.H. Warner, *Nanoscale* **5**, 4079 (2013).
9. A.W. Robertson, C.S. Allen, Y.A. Wu, K. He, J. Olivier, J. Neethling, A.I. Kirkland, J.H. Warner, *Nat. Commun.* **3**, 1144 (2012).
10. J.A. Rodriguez-Manzo, F. Banhart, *Nano Lett.* **9**, 2285 (2009).
11. J.A. Rodríguez-Manzo, O. Cretu, F. Banhart, *ACS Nano* **4**, 3422 (2010).
12. C. Jin, F. Lin, K. Suenaga, S. Iijima, *Phys. Rev. Lett.* **102**, 195505 (2009).
13. H.-P. Komsa, J. Kotakoski, S. Kurasch, O. Lehtinen, U. Kaiser, A.V. Krasheninnikov, *Phys. Rev. Lett.* **109**, 035503 (2012).
14. H.-P. Komsa, S. Kurasch, O. Lehtinen, U. Kaiser, A.V. Krasheninnikov, *Phys. Rev. B: Condens. Matter* **88**, 035301 (2013).
15. X. Liu, T. Xu, X. Wu, Z. Zhang, J. Yu, H. Qiu, J.-H. Hong, C.-H. Jin, J.-X. Li, X.-R. Wang, L.-T. Sun, W. Guo, *Nat. Commun.* **4**, 1776 (2013).
16. J.C. Meyer, A. Chuvilin, G. Algara-Siller, J. Biskupek, U. Kaiser, *Nano Lett.* **9**, 2683 (2009).
17. H. Qiu, T. Xu, Z. Wang, W. Ren, H. Nan, Z. Ni, Q. Chen, S. Yuan, F. Miao, F. Song, G. Long, Y. Shi, L. Sun, J. Wang, X. Wang, *Nat. Commun.* **4**, 2642 (2013).
18. J.C. Meyer, F. Eder, S. Kurasch, V. Skakalova, J. Kotakoski, H.J. Park, S. Roth, A. Chuvilin, S. Eyhusen, G. Benner, A.V. Krasheninnikov, U. Kaiser, *Phys. Rev. Lett.* **108**, 196102 (2012).
19. A. Chuvilin, J.C. Meyer, G. Algara-Siller, U. Kaiser, *New J. Phys.* **11**, 083019 (2009).
20. C. Jin, H. Lan, L. Peng, K. Suenaga, S. Iijima, *Phys. Rev. Lett.* **102**, 205501 (2009).
21. L. He, T. Xu, J. Sun, K. Yin, X. Xie, L. Ding, H. Xiu, L. Sun, *Carbon* **50**, 2845 (2012).
22. W. Neng, X. Jun, X. Tao, M. Martini, S. Li-tao, S. Jun, Z. Yi-long, *RSC Adv.* **3**, 17860 (2013).
23. T. Xu, X. Xie, L. Sun, *8th Annual IEEE International Conference on Nano/Micro Engineered and Molecular Systems* (IEEE Press: Piscataway, NJ, 2013), p. 637.
24. T. Xu, X. Xie, K. Yin, J. Sun, L. He, L. Sun, *Small* **10**, 1724 (2014).
25. T. Xu, K. Yin, X. Xie, L. He, B. Wang, L. Sun, *Small* **8**, 3422 (2012).
26. J. Lin, O. Cretu, W. Zhou, K. Suenaga, D. Prasai, K.I. Bolotin, N.T. Cuong, M. Otani, S. Okada, A.R. Lupini, J.-C. Idrobo, D. Caudel, A. Burger, N.J. Ghimire, J. Yan, D.G. Mandrus, S.J. Pennycook, S.T. Pantelides, *Nat. Nanotechnol.* **9**, 436 (2014).
27. W. Neng, L.-T. Sun, X.-H. Hu, Y.-Y. Zhu, Z. Lin, X. Tao, H.-C. Bi, S. Jun, F.-Z. Dong, *Cryst. Growth Des.* **12**, 3899 (2012).
28. F. Banhart, *Rep. Prog. Phys.* **62**, 1181 (1999).
29. J. Chen, T. Shi, T. Cai, T. Xu, L. Sun, X. Wu, D. Yu, *Appl. Phys. Lett.* **102**, 103107 (2013).
30. L. Li, S. Reich, J. Robertson, *Phys. Rev. B* **72**, 184109 (2005).
31. A.V. Krasheninnikov, F. Banhart, *Nat. Mater.* **6**, 723 (2007).
32. C.J. Russo, J.A. Golovchenko, *Proc. Natl. Acad. Sci. U.S.A.* **109**, 5953 (2012).
33. J.C. Meyer, C. Kisielowski, R. Erni, M.D. Rossell, M.F. Crommie, A. Zettl, *Nano Lett.* **8**, 3582 (2008).
34. A.W. Robertson, B. Montanari, K. He, C.S. Allen, Y.A. Wu, N.M. Harrison, A.I. Kirkland, J.H. Warner, *ACS Nano* **7**, 4495 (2013).
35. J. Lee, W. Zhou, S.J. Pennycook, J.-C. Idrobo, S.T. Pantelides, *Nat. Commun.* **4**, 1650 (2013).
36. W. Zhou, M.D. Kapetanakis, M.P. Prange, S.T. Pantelides, S.J. Pennycook, J.-C. Idrobo, *Phys. Rev. Lett.* **109**, 206803 (2012).
37. A.W. Robertson, B. Montanari, K. He, J. Kim, C.S. Allen, Y.A. Wu, J. Olivier, J. Neethling, N. Harrison, A.I. Kirkland, J.H. Warner, *Nano Lett.* **13**, 1468 (2013).
38. A. Krasheninnikov, P. Lehtinen, A. Foster, R. Nieminen, *Chem. Phys. Lett.* **418**, 132 (2006).
39. J. Kotakoski, A. Krasheninnikov, K. Nordlund, *Phys. Rev. B: Condens. Matter* **74**, 245420 (2006).
40. J. Kotakoski, A. Krasheninnikov, U. Kaiser, J. Meyer, *Phys. Rev. Lett.* **106**, 105505 (2011).
41. F.R. Eder, J. Kotakoski, U. Kaiser, J.C. Meyer, *Sci. Rep.* **4**, 4060 (2014).
42. J.H. Warner, E.R. Margine, M. Mukai, A.W. Robertson, F. Giustino, A.I. Kirkland, *Science* **337**, 209 (2012).
43. A. Hashimoto, K. Suenaga, A. Gloter, K. Urita, S. Iijima, *Nature* **430**, 870 (2004).
44. O. Lehtinen, S. Kurasch, A.V. Krasheninnikov, U. Kaiser, *Nat. Commun.* **4**, 2098 (2013).
45. O.V. Yazyev, S.G. Louie, *Phys. Rev. B: Condens. Matter* **81**, 195420 (2010).
46. B.W. Jeong, J. Ihm, G.-D. Lee, *Phys. Rev. B: Condens. Matter* **78**, 165403 (2008).
47. Ç.Ö. Girit, J.C. Meyer, R. Erni, M.D. Rossell, C. Kisielowski, L. Yang, C.-H. Park, M.F. Crommie, M.L. Cohen, S.G. Louie, A. Zettl, *Science* **323**, 1705 (2009).
48. B. Song, G.F. Schneider, Q. Xu, G. Pandraud, C. Dekker, H. Zandbergen, *Nano Lett.* **11**, 2247 (2011).
49. J.H. Warner, M.H. Rummeli, L. Ge, T. Gemming, B. Montanari, N.M. Harrison, B. Buchner, G.A.D. Briggs, *Nat. Nanotechnol.* **4**, 500 (2009).
50. K. Kim, S. Coh, C. Kisielowski, M.F. Crommie, S.G. Louie, M.L. Cohen, A. Zettl, *Nat. Commun.* **4**, 2723 (2013).
51. R. Zan, Q.M. Ramasse, U. Bangert, K.S. Novoselov, *Nano Lett.* **12**, 3936 (2012).
52. K. He, G.-D. Lee, A.W. Robertson, E. Yoon, J.H. Warner, *Nat. Commun.* **5**, 3040 (2014).
53. P. Koskinen, S. Malola, H. Häkkinen, *Phys. Rev. B: Condens. Matter* **80**, 073401 (2009).
54. Z. Liu, K. Suenaga, P.J.F. Harris, S. Iijima, *Phys. Rev. Lett.* **102**, 015501 (2009).
55. O. Cretu, A.R. Botello-Mendez, I. Janowska, C. Pham-Huu, J.-C. Charlier, F. Banhart, *Nano Lett.* **13**, 3487 (2013).
56. A.V. Krasheninnikov, K. Nordlund, J. Keinonen, *Phys. Rev. B: Condens. Matter* **65**, 165423 (2002).
57. J.H. Warner, Y. Fan, A.W. Robertson, K. He, E. Yoon, G.D. Lee, *Nano Lett.* **13**, 4937 (2013).
58. A.W. Robertson, K. He, A.I. Kirkland, J.H. Warner, *Nano Lett.* **14**, 908 (2014).
59. A. Chuvilin, U. Kaiser, E. Bichoutskaia, N.A. Besley, A.N. Khlobystov, *Nat. Chem.* **2**, 450 (2010).
60. J. Kotakoski, C. Mangler, J.C. Meyer, *Nat. Commun.* **5**, 3991 (2014).
61. A.W. Robertson, G.-D. Lee, K. He, E. Yoon, A.I. Kirkland, J.H. Warner, *Nano Lett.* **14**, 1634 (2014).
62. S. Kurasch, J. Kotakoski, O. Lehtinen, V. Skákalová, J. Smet, C.E. Krill, A.V. Krasheninnikov, U. Kaiser, *Nano Lett.* **12**, 3168 (2012).
63. H. Wang, Q. Wang, Y. Cheng, K. Li, Y. Yao, Q. Zhang, C. Dong, P. Wang, U. Schwingenschlögl, W. Yang, X.X. Zhang, *Nano Lett.* **12**, 141 (2012).
64. J. Zhao, Q. Deng, A. Bachmatiuk, G. Sandeep, A. Popov, J. Eckert, M.H. Rümmeli, *Science* **343**, 1228 (2014).
65. F. Banhart, *Nanoscale* **1**, 201 (2009).
66. Y. Gan, L. Sun, F. Banhart, *Small* **4**, 587 (2008).
67. Z. He, K. He, A.W. Robertson, A.I. Kirkland, D. Kim, J. Ihm, E. Yoon, G.-D. Lee, J.H. Warner, *Nano Lett.* **14**, 3766 (2014).
68. J.A. Rodríguez-Manzo, C. Pham-Huu, F. Banhart, *ACS Nano* **5**, 1529 (2011).
69. O. Cretu, J.A. Rodríguez-Manzo, A. Demortière, F. Banhart, *Carbon* **50**, 259 (2012).
70. O. Cretu, A.V. Krasheninnikov, J.A. Rodriguez-Manzo, L.T. Sun, F. Banhart, R.M. Nieminen, *Phys. Rev. Lett.* **105**, 196102 (2010).
71. W.L. Wang, E. Santos, B. Jiang, E. Cubuk, C. Ophus, A. Centeno, A. Pesquera, A. Zurutuza, J. Ciston, R.M. Westervelt, *Nano Lett.* **14**, 450 (2014).
72. H. Wang, K. Li, Y. Cheng, Q. Wang, Y. Yao, U. Schwingenschlögl, X. Zhang, W. Yang, *Nanoscale* **4**, 2920 (2012).
73. R. Erni, M.D. Rossell, M.-T. Nguyen, S. Blankenburg, D. Passerone, P. Hartel, N. Alem, K. Erickson, W. Gannett, A. Zettl, *Phys. Rev. B: Condens. Matter* **82**, 165443 (2010).
74. J.H. Warner, Z. Liu, K. He, A.W. Robertson, K. Suenaga, *Nano Lett.* **13**, 4820 (2013).
75. A. Krasheninnikov, P. Lehtinen, A. Foster, P. Pyykkö, R. Nieminen, *Phys. Rev. Lett.* **102**, 126807 (2009).
76. N. Alem, R. Erni, C. Kisielowski, M.D. Rossell, W. Gannett, A. Zettl, *Phys. Rev. B: Condens. Matter* **80**, 155425 (2009).
77. J. Kotakoski, C. Jin, O. Lehtinen, K. Suenaga, A. Krasheninnikov, *Phys. Rev. B: Condens. Matter* **82**, 113404 (2010).

https://doi.org/10.1557/mrs.2014.303 Published online by Cambridge University Press

78. A. Zobelli, A. Gloter, C. Ewels, G. Seifert, C. Colliex, *Phys. Rev. B: Condens. Matter* **75**, 245402 (2007).
79. O. Cretu, Y.-C. Lin, K. Suenaga, *Nano Lett.* **14**, 1064 (2014).
80. A.L. Gibb, N. Alem, J.-H. Chen, K.J. Erickson, J. Ciston, A. Gautam, M. Linck, A. Zettl, *J. Am. Chem. Soc.* **135**, 6758 (2013).
81. J.H. Warner, M.H. Rümmeli, A. Bachmatiuk, B. Büchner, *ACS Nano* **4**, 1299 (2010).
82. X. Wei, M.-S. Wang, Y. Bando, D. Golberg, *ACS Nano* **5**, 2916 (2011).
83. O.L. Krivanek, M.F. Chisholm, V. Nicolosi, T.J. Pennycook, G.J. Corbin, N. Dellby, M.F. Murfitt, C.S. Own, Z.S. Szilagyi, M.P. Oxley, S.T. Pantelides, S.J. Pennycook, *Nature* **464**, 571 (2010).
84. L. Ci, L. Song, C. Jin, D. Jariwala, D. Wu, Y. Li, A. Srivastava, Z.F. Wang, K. Storr, L. Balicas, F. Liu, P.M. Ajayan, *Nat. Mater.* **9**, 430 (2010).
85. L.P. Hansen, Q.M. Ramasse, C. Kisielowski, M. Brorson, E. Johnson, H. Topsøe, S. Helveg, *Angew. Chem., Int. Ed.* **50**, 10153 (2011).
86. Z. Liu, K. Suenaga, Z. Wang, Z. Shi, E. Okunishi, S. Iijima, *Nat. Commun.* **2**, 213 (2011).
87. Y.-C. Lin, D.O. Dumcenco, Y.-S. Huang, K. Suenaga, *Nat. Nanotechnol.* **9**, 391 (2014).
88. R. Zan, Q.M. Ramasse, R. Jalil, T. Georgiou, U. Bangert, K.S. Novoselov, *ACS Nano* **7**, 10167 (2013).
89. G. Algara-Siller, S. Kurasch, M. Sedighi, O. Lehtinen, U. Kaiser, *Appl. Phys. Lett.* **103**, 203107 (2013).
90. W. Zhou, M.D. Kapetanakis, M.P. Prange, S.T. Pantelides, S.J. Pennycook, J.-C. Idrobo, *Phys. Rev. Lett.* **109**, 206803 (2012). □





https://doi.org/10.1557/mrs.2014.303 Published online by Cambridge University Press